CSEM quantitative interpretation for reservoir property estimation and anti-model evaluation

Jan Petter Morten, Jon Olav Jenssen, Elias Andre Nerland, and Pål T. Gabrielsen, EMGS ASA; John Reidar Granli, OMV Norway*

Summary

We have developed a workflow for quantitative interpretation of CSEM data. The interpretation method utilizes that CSEM responses are determined by the product of resistivity-contrast and thickness for hydrocarbon reservoirs and resistive lithologies. This enables exhaustive investigation of rock physics models supporting the measurements, and uncertainty estimation in the property domain. The properties that can be estimated are e.g. hydrocarbon volume and gross thickness of the hydrocarbon saturated column. The property and column predictions are on the reservoir scale and can be directly evaluated in conjunction with thickness estimates from seismic. Our approach is also suited for evaluation of anti-models as the cause for a resistor. This analysis can support interpretation of a resistor mapped using CSEM and give input to risking. We illustrate the workflow and discuss resistor causation using Barents Sea examples and compare predictions to drilling results for a fluid case and a tight-reservoir case.

Introduction

Full realization of the value potential of controlled source electromagnetic (CSEM) data relies on effective integration that enables reliable extraction of reservoir properties from the data with the interpreter in the "driving seat". This objective is difficult to achieve in part because of the technically challenging nature of the imaging that is used. This is full waveform inversion, and requires specialist knowledge, i.e. understanding of regularization and the non-unique solution space of the inverse problem. However, significant advances have been realized by the introduction of more powerful update schemes and integration with other geophysical data at the inversion stage (Nguyen et al., 2016; Colombo and Rovetta, 2018) as well as post-inversion interpretation analysis using 3D modeling.

A good 3D inversion result determines the resistivity distribution and identifies zones of anomalous high resistivity. Assessment of sensitivity and imaging robustness can further establish the uncertainty of the resistor properties. While such analysis can derisk a hydrocarbon reservoir prospect, interpretation must also consider other possible origins of the high resistivity, i.e. "anti-models". We propose to use quantitative interpretation as a tool to attain further information about the possible resistive scenarios. By considering how the invariant part of the CSEM result for a resistor can be transformed into rock properties for different rock physics models, it becomes possible to test whether e.g. the thickness of the resistive lithology or hydrocarbon saturated reservoir rock is compatible with seismic mapped thickness.

Our analysis will be formulated in terms of the resistivity-contrast times thickness for a thin horizontal resistor, also known as the anomalous transverse resistance (ATR). This quantity is the underlying parameter that determines the CSEM response (Constable and Weiss, 2006). This has been confirmed both by theoretical investigations (Mittet and Morten, 2013) and by field data comparison with downhole measurements (Morten et al., 2017).

The large computational requirements for 3D CSEM inversion means that only a very limited number of attempts varying e.g. the input data content, parameterization, and regularization can be executed in one project. This currently prohibits full investigation of the non-unique solution. However, a large class of non-unique resistor properties pertain to variation of burial depth and thickness due to the low resolution of the low-frequency data. Therefore, the representation in terms of ATR captures a lot of the ambiguity, i.e. the ATR will be similar for the realizations of a resistor that are confined to the depth window used for the ATR extraction. In our approach, the ATR from inversion is analyzed in a second stage and mapped to reservoir properties according to rock physics models. This operation is very fast and allows interactive investigation of the solution space in the reservoir/rock properties domain. While the inversion process may be a task for CSEM inversion experts, this subsequent property mapping is available to a wide group of interpreters.

Rock physics framework

The ATR can be computed from a CSEM 3D resistivity cube by numerical integration in the vertical direction over a depth window defined by seismic structure. Alternatively, more advanced constrained inversion approaches can be employed to achieve higher accuracy. The ATR property is not limited to CSEM; it can easily also be computed from the rock physics relationships, and this facilitates a link between the domains. From rock physics, we compute

$$\mathrm{ATR}(x,y) = \int_{h_0(x,y)}^{h(x,y)} (R_\mathrm{V}(x,y,z) - R_\mathrm{B})\, dz\ . \qquad (1)$$

In this expression, R_V is the vertical resistivity, R_B is background resistivity, h_0 and h are the base and top depth of the reservoir or resistive lithology. The rock physics model will be embodied in R_V. This function will typically depend on depth (z). The relationship between ATR and

10.1190/segam2019-3214693.1

resistor thickness, $h - h_0$, can be tabulated quickly using quadrature.

We have implemented a shaley sand rock physics model to represent the resistivity effect of hydrocarbon saturation. A range of different models are described by Mavko et al. (2009) which can be expressed as the "parallel coupling" of a resistor parameterized by the Archie equation and conduction depending on distributed clay,

$$\frac{1}{R_\mathrm{t}} = \frac{1}{a\phi^{-m}S_\mathrm{W}^{-n}R_\mathrm{W}} + X. \qquad (2)$$

In this equation, R_t is the isotropic rock resistivity, a is tortuosity, ϕ is effective porosity, m is cementation exponent, S_W is brine saturation, n is saturation exponent, R_W is brine resistivity, and X represents the conduction effect of distributed clay. A simple model is $X = V_\mathrm{cl}\sigma_\mathrm{cl}$ (Simandoux, 1963) which represents this conduction by a volume fraction and a conductivity. The saturation is condition to $S_\mathrm{W} + S_\mathrm{HC} = 1$ where S_HC is the hydrocarbon saturation. In this model we do not distinguish between oil and gas saturations but assume an approximately similar effect on resistivity. The opposing effects of buoyancy and capillary forces result in a transition zone in a hydrocarbon reservoir where the water saturation develops from 100 % close to the oil-water-contact (OWC) towards the irreducible water saturation $S_\mathrm{W,irr}$. We model the resulting depth-dependence using the following expression,

$$S_\mathrm{W}(z) = \left(1 - S_\mathrm{W,irr}\right)\mathrm{e}^{-z/l} + S_\mathrm{W,irr}, \qquad (3)$$

where l is the scale parameter for the transition zone which will depend on pore throat radius and fluid density (Skelt, 1996). In this expression we referenced OWC depth to $z = 0$ with z positive up. The relationship between ATR and hydrocarbon saturated column height can now be determined from (1)-(3). Note that similar integrals as (1) relate ATR to hydrocarbon pore column HCPC $= \int \phi S_\mathrm{HC} dz$ which is useful for computing volumetrics.

We extend the model to represent reservoirs with layers of non-reservoir rock, quantified by the net-to-gross (NTG) ratio. The non-reservoir rock is introduced as intervals of integration in (1) with a fixed vertical resistivity $R_\mathrm{non-res}$. The parameters in the rock physics model will typically be calibrated to well data interpretations for reservoirs assumed analogue to the target under investigation. To describe uncertainty in the parameters resulting from such extrapolation, the software facilitates representation of parameters by a probability distribution, which is used for stochastic simulation of the ATR relationships. The results are analyzed as P10, P50, and P90 percentiles of the simulated cumulative probability distribution. As an example, Figure 1 shows results from a model with parameters calibrated to the Stø reservoir level encountered in the well 7324/7-2 close to the Wisting discovery in the Barents Sea, Norway. To evaluate a target in the same formation but with assumed deteriorated reservoir quality, we introduced a uniform probability distribution for NTG between 70-100 %. Further, we model the reservoir layers thickness as lognormal distributed with mode of 8 m. The irreducible water saturation 4 % is reached at approximately $3l = 12$ m height in this model, where the peak resistivity 1.8 kΩm is reached. The simulated P50 results with NTG distribution have an ATR of about 11 $k\Omega\mathrm{m}^2$ for a 20 m gross hydrocarbon saturated reservoir column. The distribution has a wide spread below the mean due to realizations where non-reservoir layers occupy the upper part of the column where the dominating contribution to ATR at $S_\mathrm{W,irr}$ is missed. Uncertainty in the ATR can also be studied in our formalism, but we note that typically it is uncertainty in the rock physics model parameters that give dominating contribution to the uncertainty in thickness and volume predictions.

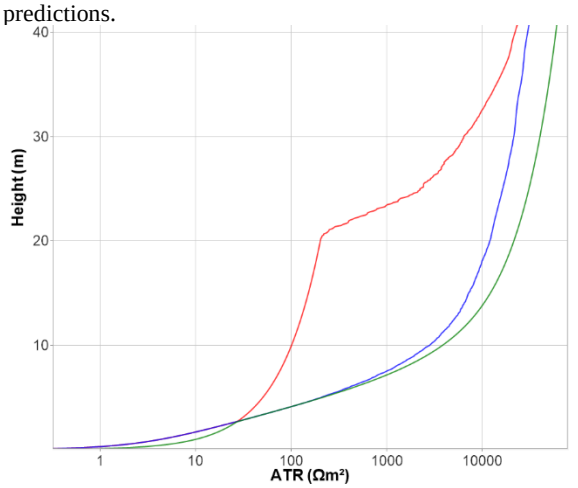

Figure 1 Relationship between ATR and hydrocarbon saturated column height from stochastic modeling. The cumulative probability distribution is presented in terms of 10 (red),50 (blue), and 90 (green) percentiles.

The model in (2) can also be used to study cemented sandstone anti-model scenarios for a resistive prospect. Such lithology will be high-resistive due to low porosity and high cementation exponent but have $S_\mathrm{W} = 1$. The interpretation of ATR will then focus on predicting the thickness of the cemented reservoir layer. Other types of resistive anti-models can also be accommodated, for example fresh-water layers (low salinity, high R_W) and hydrates. The scheme can also incorporate other types of rock physics models that describe resistive lithologies, for example source rocks with variable maturity and organic carbon content.

Case 1: "Gemini North" 7325/4-1

The deployment of CSEM technology in the Hoop area of the Barents Sea has been very successful, and is described in

10.1190/segam2019-3214693.1

several papers (Granli et al., 2017; Alvarez et al., 2017). Doubtless this success is related to the shallow burial depth and high-resistive targets which are ideal for characterization using CSEM. The area licensed as PL855 was surveyed using high-resolution CSEM and seismic, and the pre-drill assessment and well outcome using CSEM was described by Granli et al. (2018).

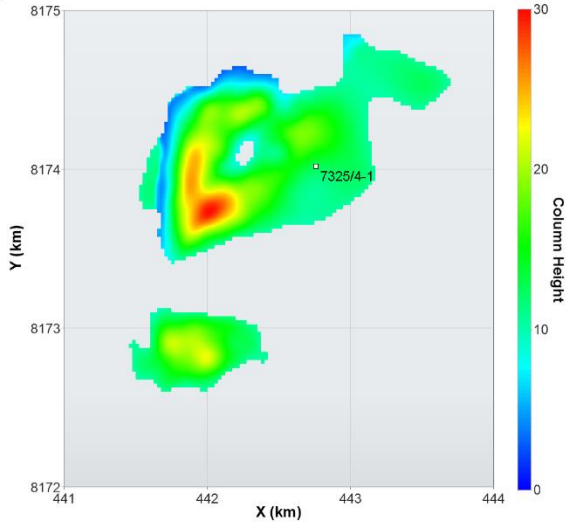

Figure 2 HC saturated column height prediction at Gemini North.

Figure 2 shows the prediction of hydrocarbon saturated column height for the area. The map was calculated using ATR from constrained 3D CSEM inversion by the formalism and well calibration described above. We also used a base reservoir interpretation from seismic to determine the surface denoted h_0 in (1). At the gas discovery well position, the predicted column height is 13 m. This prediction can be compared to the well outcome shown in Figure 3. The well showed that the Stø reservoir is comprised of two levels with different reservoir quality. The upper level is about 6.5 m thick and has a considerably lower resistivity than the lower level that is about 13.5 m thick. With respect to ATR it is the lower level that dominates the contribution, and the lower level was found to have similar electrical resistivity properties as the calibration well used in this study. This prompts the excellent agreement with the CSEM prediction. When applying the model that incorporates the NTG probability distribution described above and shown in Figure 1, the P50 gross column thickness prediction is very close to the well outcome for total thickness of hydrocarbon saturated Stø.

Case 2: "Koigen" 7317/9-1

We will now apply the quantitative interpretation methodology to investigate a resistor in the area licensed as PL718 in the Stappen High region of the Barents Sea. The primary exploration target for the well, 7319-91, was to prove petroleum in Middle Jurassic to Late Triassic reservoir rocks (the Realgrunnen sub-group). The secondary target was in Late – to Middle Triassic reservoir rocks (Tubåen and Snadd formation). The well encountered multiple sandstone layers in both exploration targets. All sandstones are reported to have poor to no reservoir quality and the well is classified as a dry well.

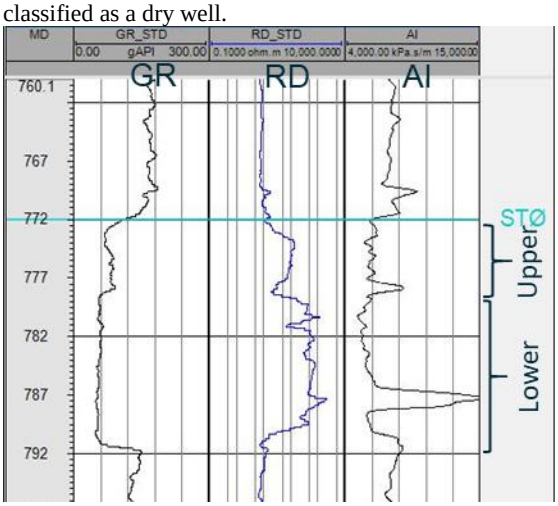

Figure 3 Well logs from 7325/4-1 from left to right: Gamma, deep resistivity, acoustic impedance. The Stø interval is composed of two types of reservoir, here denoted as "upper" and "lower".

The 3D CSEM data was acquired in 2012 using a 3 km × 3 km staggered receiver grid with some additional crossline source towing. The transmitted waveform has frequency range 0.9 - 10.5 Hz providing good sensitivity to both target intervals. The 3D inversion did not use any a priori information, and images a large resistor with very high ATR values that is partly structurally conforming (Figure 4).

Let us now consider a pre-drill interpretation scenario. Earlier results from exploration well 7318/12-2 are assumed relevant. This well encountered tight and high-resistive reservoir that was interbedded with conductive shale. To reflect this risk, we construct a reservoir model with $\phi = 3\ \%$ and $m = 2.4$ to model the resistive lithology. In addition, a fluid case will also be evaluated using a rock physics model with parameters like those calibrated to Wisting area wells and NTG = 90 %. Figure 5 shows the relationship between the resistor height and ATR for the two scenarios. The ATR effect for the two models is similar.

10.1190/segam2019-3214693.1

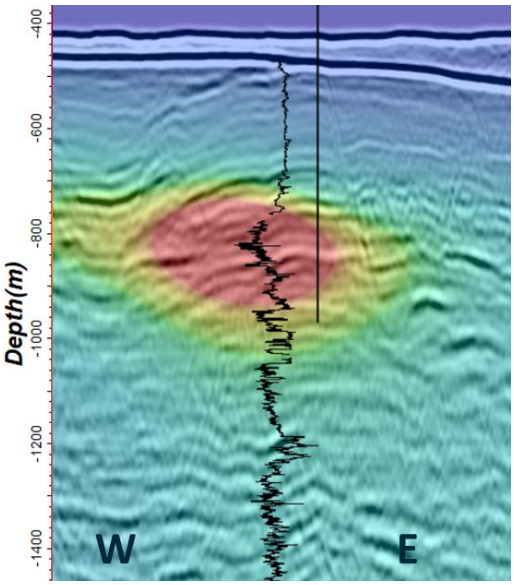

Figure 4 Co-visualization of resistivity well log 7317/9-1, seismic, and CSEM vertical resistivity. Seismic data courtesy of TGS.

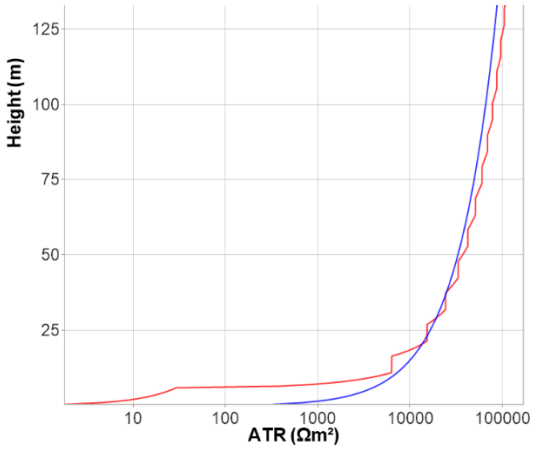

Figure 5 ATR versus thickness for two different scenarios for the origin of the resistor: Hydrocarbon saturated reservoir (red) and cemented sandstone (blue).

The ATR from 3D unconstrained inversion was used in the formalism described in this paper to predict resistor thickness at the well location. The prediction from the fluid model is 81 m hydrocarbon saturated reservoir thickness. The cemented sandstone anti-model leads to a prediction of 109 m thick lithology (Figure 6). Given the uncertainty of the input rock physics parameters, we may conclude that both a fluid scenario and a resistive lithology scenario can be supported by the CSEM data. Comparison of these predictions to the thickness mapped from seismic may lead to a preference of one of the cases.

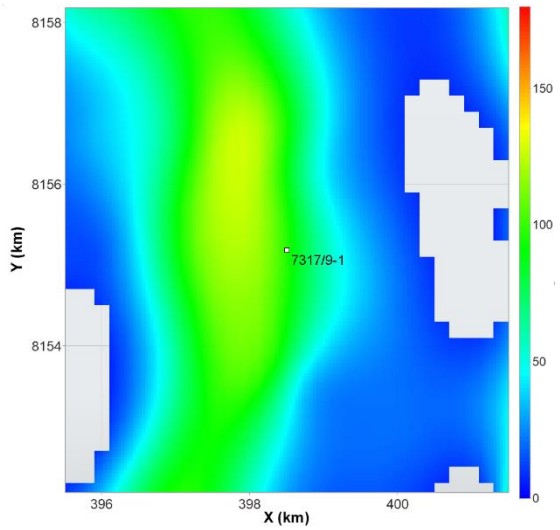

Figure 6 Color code shows predicted cemented sand thickness using the Archie equation with porosity 3% and cementation exponent 2.4. At the well position, the thickness is 109 m.

The well outcome as described in the press release is dry, encountering two reservoir zones with "very poor reservoir quality". This represents cemented high-resistive sandstones. The combined reservoir thickness was reported as 110 m, in good agreement with the prediction described above for the cemented sandstone case. Due to limited resolution, the CSEM data does not resolve the two layers individually but captures the combined effect.

Conclusions

We have described a framework for quantitative interpretation of CSEM data. Our scheme embraces the transverse resistance equivalence which acts as a natural upscaling operator in this context. The methodology was demonstrated for two very different areas and compared to well results. The framework is equally applicable to analyze fluid and lithology on resistivity. By quantifying properties of the target for comparison to other information for example seismic mapped thickness, such quantitative methods can aid to distinguish these to de-risk drilling CSEM mapped resistors. Further developments of this methodology will focus on integration with quantitative seismic interpretation results and estimated facies to define 3D rock physics models with variable properties.

Acknowledgments

We thank EMGS ASA, OMV Norway, and the PL855 license partners Equinor and Petoro for permission to publish these results.

10.1190/segam2019-3214693.1

REFERENCES

Alvarez, P., A. Alvarez, L. Macgregor, F. Bolivar, R. Keirstead, and T. Martin, 2017, Reservoir properties integrating controlled-source electromagnetic, prestack seismic and well log data using a rock-physics framework: Case study in the hoop Area, Barents Sea, Norway: Interpretation, **5**, SE43–SE60, doi: https://doi.org/10.1190/INT-2016-https://doi.org/0097.1.

Colombo, D., and D. Rovetta, 2018, Geophysical joint inversion with multiple coupling operators: 88th Annual International Meeting, SEG, Expanded Abstracts, 2292–2296, doi: https://doi.org/10.1190/segam2018-2984464.1

Constable, S., and C. J. Weiss, 2006, Mapping thin resistors and hydrocarbons with marine EM methods: Insights from 1D modeling: Geophysics, **71**, G43–G51, doi: https://doi.org/10.1190/1.2187748.

Granli, J. R., D. Daudina, S. C. Robertson, J. P. Morten, P. T. Gabrielsen, and B. Sigvathsen, 2018, Applying high-resolution 3D CSEM and seismic for integrated reservoir characterization: 88th Annual International Meeting, SEG, Expanded Abstracts, 949–953, doi: https://doi.org/10.1190/segam2018-2995351.1.

Granli, J. R., H. H. Veire, P. T. Gabrielsen, and J. P. Morten, 2017, Maturing broadband 3D CSEM for improved reservoir property prediction in the Realgrunnen Group at Wisting, Barents Sea: 87th Annual International Meeting, SEG, Expanded Abstracts, 2205–2209, doi: https://doi.org/10.1190/segam2017-17727091.1.

Mavko, G., T. Mukerji, and J. Dvorkin, 2009, The rock physics handbook: Cambridge University Press.

Mittet, R., and J. P. Morten, 2013, The marine controlled-source electromagnetic method in shallow water: Geophysics, **78**, E67–E77, doi: https://doi.org/10.1190/geo2012-0112.1.

Morten, J. P., H. H. Veire, J. R. Granli, and P. T. Gabrielsen, 2017, Quantitative comparison of deep-reading well resistivity to 3D CSEM at Wisting: 87th Annual International Meeting, SEG, Expanded Abstracts, 1174–1178, doi: https://doi.org/10.1190/segam2017-17723740.1.

Nguyen, A. K., J. I. Nordskag, T. Wiik, A. Kornberg Bjørke, L. Boman, O. M. Pedersen, J. Ribaudo, and R. Mittet, 2016, Comparing large-scale 3D Gauss-Newton and BFGS CSEM inversions: 86th Annual International Meeting, SEG, Expanded Abstracts, 872–877, doi: https://doi.org/10.1190/segam2016-13858633.1.

Simandoux, P., 1963, Dielectric measurements on porous media: Application to the measurement of water saturations: study of the behavior of argillaceous formations: Revue de l'Institut Francais du Petrole, **18**, 193–215.

Skelt, C., 1996, A relationship between height, saturation, permeability and porosity: Presented at the SPWLA 17th European Formation Evaluation Symposium, E018.